Cell Reports
Report

Genetic Reduction of the α1 Subunit of Na/K-ATPase Corrects Multiple Hippocampal Phenotypes in Angelman Syndrome

Hanoch Kaphzan,[1,2] Shelly A. Buffington,[3] Akila B. Ramaraj,[1] Jerry B. Lingrel,[4] Matthew N. Rasband,[3] Emanuela Santini,[1] and Eric Klann[1,*]
[1]Center for Neural Science, New York University, New York, NY 10003, USA
[2]Sagol Department of Neurobiology, University of Haifa, Haifa 3190501, Israel
[3]Department of Neuroscience, Baylor College of Medicine, Houston, TX 77030, USA
[4]Department of Molecular Genetics, Biochemistry and Microbiology, University of Cincinnati, Cincinnati, OH 45267, USA
*Correspondence: eklann@cns.nyu.edu
http://dx.doi.org/10.1016/j.celrep.2013.07.005

SUMMARY

Angelman syndrome (AS) is associated with symptoms that include autism, intellectual disability, motor abnormalities, and epilepsy. We recently showed that AS model mice have increased expression of the alpha1 subunit of Na/K-ATPase (α1-NaKA) in the hippocampus, which was correlated with increased expression of axon initial segment (AIS) proteins. Our developmental analysis revealed that the increase in α1-NaKA expression preceded that of the AIS proteins. Therefore, we hypothesized that α1-NaKA overexpression drives AIS abnormalities and that by reducing its expression these and other phenotypes could be corrected in AS model mice. Herein, we report that the genetic normalization of α1-NaKA levels in AS model mice corrects multiple hippocampal phenotypes, including alterations in the AIS, aberrant intrinsic membrane properties, impaired synaptic plasticity, and memory deficits. These findings strongly suggest that increased expression of α1-NaKA plays an important role in a broad range of abnormalities in the hippocampus of AS model mice.

INTRODUCTION

Angelman syndrome (AS) is a neurodevelopmental disorder characterized by autism, mental retardation, absence of speech, motor abnormalities, and epilepsy (Lossie et al., 2001; Williams et al., 2006). In most cases, AS is caused by the deletion of small portions on the maternal copy of chromosome 15, which includes the *UBE3A* gene (Kishino et al., 1997; Knoll et al., 1989; Matsuura et al., 1997; Sutcliffe et al., 1997). *UBE3A* encodes the ubiquitin ligase E3A (also termed E6-AP), which covalently attaches polyubiquitin chains to proteins, resulting in their degradation by the 26S proteasome. AS model mice exhibit multiple levels of brain dysfunction that correlate with the neurological abnormalities observed in humans, including cognitive deficits (Jiang et al., 1998). For example, hippocampus-dependent long-term memory and long-term potentiation (LTP), a cellular model for learning and memory, have been shown to be impaired in AS model mice (Jiang et al., 1998; van Woerden et al., 2007).

Hippocampal CA1 pyramidal neurons in AS mice have altered passive and active intrinsic membrane properties (Kaphzan et al., 2011) that are correlated with the increased expression of the α1 subunit of Na/K ATPase (α1-NaKA), the voltage-gated sodium channel NaV1.6, and the axon initial segment (AIS) protein ankyrin-G, as well as increased AIS length (Kaphzan et al., 2011). In addition, it was shown that the increased expression of α1-NaKA was developmental and preceded the increased expression of NaV1.6 and ankyrin-G (Kaphzan et al., 2011). It has been shown that increased expression and activity of α1-NaKA lowers the resting membrane potential and induces a less excitable state (Brodie et al., 1987; Gadsby, 1984; Mallick et al., 2010; Silva et al., 2006). Moreover, it was shown that disrupting presynaptic input, which also decreases neuronal excitability, results in AIS changes similar to what was observed in AS model mice (Kuba et al., 2010). Therefore, we hypothesized that the increased expression of α1-NaKA in AS mice induces a decrease in neuronal excitability that drives changes at the AIS in an effort to restore neuronal excitability to levels observed in wild-type mice.

Here we report that genetic reduction of α1-NaKA prevents the electrophysiological, biochemical, and morphological abnormalities in the AIS in the hippocampus of AS model mice. In addition, the genetic reduction of α1-NaKA corrects impaired LTP and hippocampus-dependent memory deficits displayed by the AS model mice. Our findings suggest that

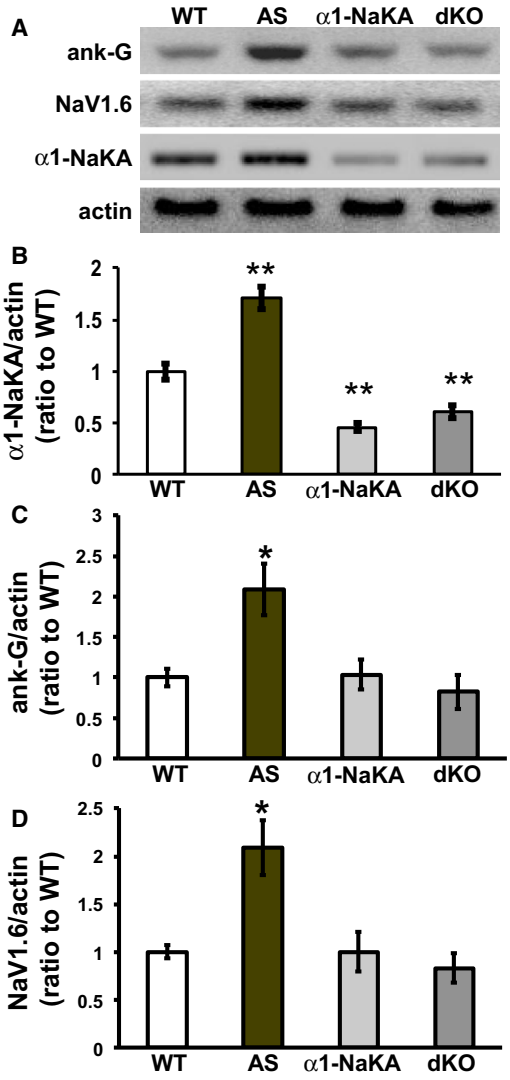

Figure 1. Genetic Reduction of α1-NaKA Corrects Increased Expression of Ankyrin-G and NaV1.6 in AS Model Mice

Western blot analysis of hippocampal homogenates from wild-type (WT), Angelman syndrome (AS), α1-NaKA heterozygous knockout (α1-NaKA), and AS/α1-NaKA heterozygous knockout (dKO) mice.

(A) Representative blots of ankyrin-G (480 kDa), NaV1.6, α1-NaKA, and actin.

(B) Cumulative data for the blots probed for α1-NaKA and actin.

(C) Cumulative data for the blots probed with antibodies to ankyrin-G and actin.

(D) Cumulative data for the blots probed for NaV1.6 and actin.

For all panels, actin was used as a loading control and quantification was done as a ratio to wild-type on the same blot (WT: n = 6; AS: n = 7; α1-NaKA: n = 7; dKO: n = 7). Asterisks (*$p < 0.05$ and **$p < 0.01$) denote statistical significance from wild-type (ANOVA followed by Tukey's post-hoc test). Results are displayed as mean ± SEM.

increased expression of α1-NaKA in early development involves altered intrinsic membrane properties, AIS pathology, impaired synaptic plasticity, and cognitive deficits in the hippocampus of AS model mice.

RESULTS

Genetic Reduction of α1-NaKA Levels Corrects Increases in the Expression of Ankyrin-G and NaV1.6 in the Hippocampus of AS Mice

In AS mice, increased expression of α1-NaKA preceded the increased expression of the AIS-related proteins, and in regions where α1-NaKA expression was not increased, the AIS was unaltered (Kaphzan et al., 2011). Therefore, we hypothesized that the increased expression of α1-NaKA drives the AIS alterations in the AS mice. To test this hypothesis, we bred female mice that carried the deletion of *Ube3A* from a paternal origin ($Ube3A^{+/-\ (m/p)}$) (so that the behavior of these females would not be affected) with male mice that were heterozygous for the deletion of α1-NaKA ($\alpha1\text{-}NaKA^{+/-\ (m/p)}$). This breeding strategy resulted in four distinct genotypes: wild-type, $Ube3A^{-/+\ (m/p)}$ (AS), $\alpha1\text{-}NaKA^{+/-\ (m/p)}$ (α1NaKA), and $Ube3A^{-/+\ (m/p)}/\alpha1\text{-}NaKA^{+/-\ (m/p)}$ double-knockout (dKO) mice.

First, we confirmed that the expression of α1-NaKA was reduced in the dKO progeny resulting from crossing the AS mice with α1-NaKA heterozygous knockout mice (Figures 1A and 1B). We then proceeded to determine whether reducing α1-NaKA levels could prevent the increase in AIS-related protein levels in the AS mice. We found that the genetic reduction of α1-NaKA expression prevented the increased expression of both ankyrin-G and NaV1.6 in AS mice, restoring them to levels observed in wild-type mice (Figures 1C and 1D). These findings are consistent with the idea that the increased expression of α1-NaKA leads to increases in the expression of ankyrin-G and NaV1.6.

AIS Length in CA1 and CA3 Pyramidal Neurons in the Hippocampus of AS Mice Is Normalized by Genetic Reduction of α1-NaKA Levels

The normalization of NaV1.6 and ankyrin-G levels in AS mice to those observed in wild-type mice by reducing α1-NaKA expression led us to determine the AIS length in the dKO mice. Consistent with the correction in ankyrin-G and NaV1.6 protein expression, the length of the AIS in hippocampal CA1 and CA3 pyramidal neurons in the AS mice with the heterozygous deletion of α1-NaKA was similar to that observed in wild-type mice (Figures 2A and 2B). The length of the AIS in hippocampal CA1 and CA3 pyramidal neurons in the α1-NaKA heterozygous knockout mice was unaltered relative to their wild-type counterparts. We previously reported that AIS length in the somatosensory cortex of AS mice was similar to that in wild-type littermates (Kaphzan et al., 2011). Here we found that the AIS length of neurons in the somatosensory cortex did not differ among the four genotypes (Figure 2C). These results suggest that increased expression of α1-NaKA leads not only to increased expression of AIS-related proteins but also alterations in AIS morphology in the hippocampus of AS mice.

Genetic Reduction of α1-NaKA Levels Corrects Altered Intrinsic Membrane Properties in Hippocampal CA1 Pyramidal Neurons in AS Mice

The increased expression of AIS-related proteins and the increase in AIS length in AS mice are correlated with altered intrinsic membrane properties in hippocampal pyramidal

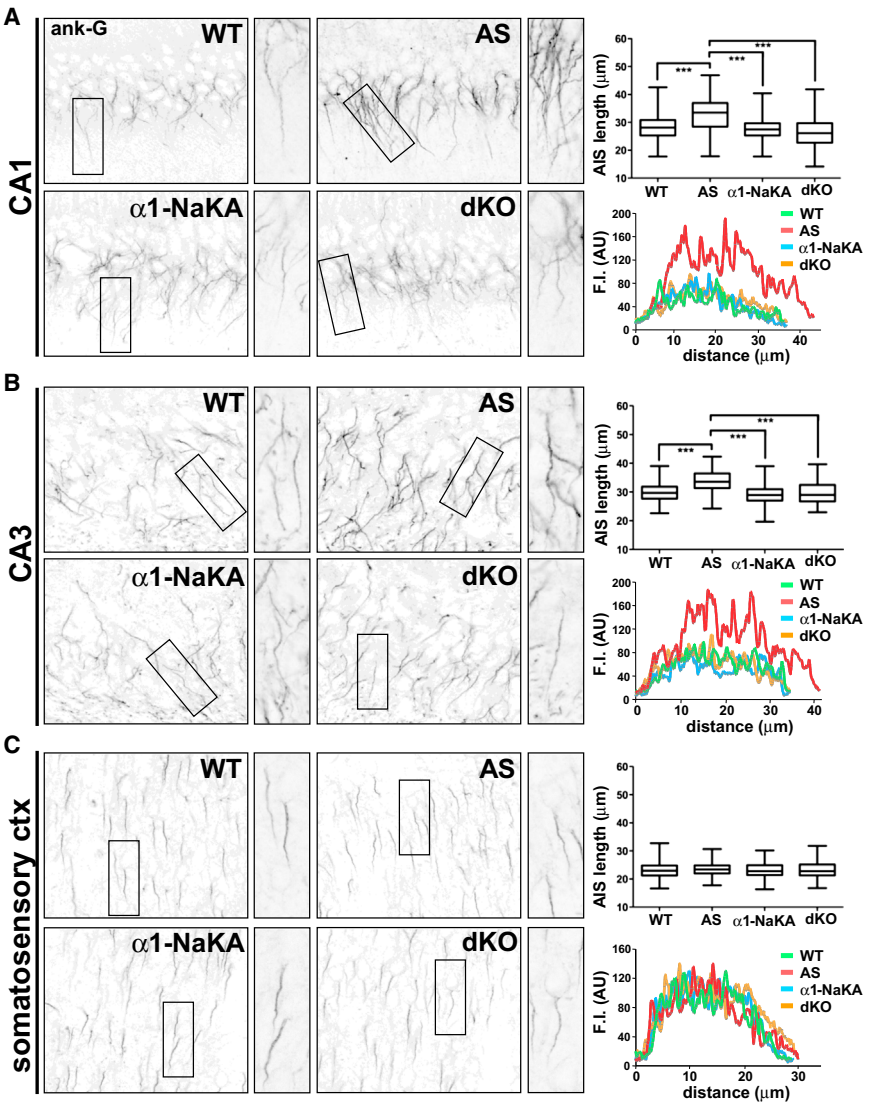

Figure 2. AIS Length in AS Model Mice Is Restored to Wild-Type Length in Hippocampal CA1 and CA3 Pyramidal Neurons by Genetically Reducing α1-NaKA Levels

(A–C) Immunostaining analysis of ankyrin-G expression and AIS length in hippocampal and cortical tissue from wild-type (WT), Angelman syndrome (AS), α1-NaKA heterozygous knockout (α1-NaKA), and AS/α1-NaKA heterozygous knockout (dKO) mice. Coronal brain slices containing the hippocampal formation and somatosensory cortex were immunostained with antibodies targeted against ankyrin-G. AIS length was quantified in CA1 (A), CA3 (B), and layer II/III somatosensory cortex (C) in tissue from each of the four genotypes. WT: n = 240 cells per region, 2 mice; AS: n = 239 cells per region, 2 mice; α1-NaKA: n = 240 cells per region, 2 mice; dKO: n = 239 cells per region, 2 mice. Average, region-specific AIS length data are provided in box and whisker plots. ***$p < 0.001$ (ANOVA). Fluorescence intensity (F.I.) plots provide a comparison of representative AIS ankyrin-G immunosignal strength and AIS length of cells contained in the expanded views, shown to the right of the contextual image.

neurons (Kaphzan et al., 2011). Therefore, we determined whether the genetic reduction of α1-NaKA could correct the altered intrinsic membrane properties in the AS mice. We found that each of the intrinsic properties that were shown to be altered in the AS mice, including resting potential, threshold potential, action potential amplitude, and the action potential maximal rate of rise, were corrected to wild-type values in the dKO mice ($p < 0.001$, ANOVA for all of the intrinsic values measured) (Figures 3A, 3D, 3E, and 3G). Other intrinsic properties that were unaltered in AS mice, including membrane time constant, input resistance, full width of action potential at half-maximum, and rheobase, remained unchanged with the heterozygous deletion of α1-NaKA (Figures 3B, 3C, 3F, and 3H). α1-NaKA heterozygous knockout mice exhibited intrinsic properties that were indistinguishable from wild-type mice. Examples of the traces of the action potentials and their derivative (as described in Experimental Procedures) for determining the action potential threshold, peak and maximal rate of rise are displayed in Figures S1A and S1B, and sample traces of current injections for acquisition of action potentials are shown Figure S1D. These results indicate that the genetic reduction of α1-NaKA corrects altered intrinsic membrane properties of hippocampal pyramidal neurons in AS mice.

Hippocampal Synaptic Plasticity and Memory Impairments Exhibited by AS Mice Are Rescued by Genetic Reduction of α1-NaKA Levels

We next determined whether the genetic reduction of α1-NaKA could correct two of the most robust hippocampal phenotypes displayed by the AS mice: impaired LTP and deficits in long-term memory (Jiang et al., 1998; van Woerden et al., 2007). Consistent with previous findings, we found that LTP was impaired in hippocampal slices from AS mice (Figure 4A). The impaired LTP in AS mice could be completely prevented by the heterozygous deletion of α1-NaKA (Figure 4A). α1-NaKA heterozygous knockout mice exhibited LTP comparable to that observed in wild-type mice (Figures 4A and 4B). Paired-pulse facilitation in the dKO mice before and after HFS was similar (Figure S2A), suggesting that the correction of LTP was achieved via a postsynaptic mechanism. These results indicate the genetic reduction of α1-NaKA can correct impaired hippocampal synaptic plasticity in AS mice.

We proceeded to examine long-term hippocampus-dependent memory in the dKO mice using contextual fear and Morris water maze (MWM) tests. The acquisition of the fear memory was similar among all four genotypes (Figure S2B), suggesting that sensory perception did not differ among the four genotypes.

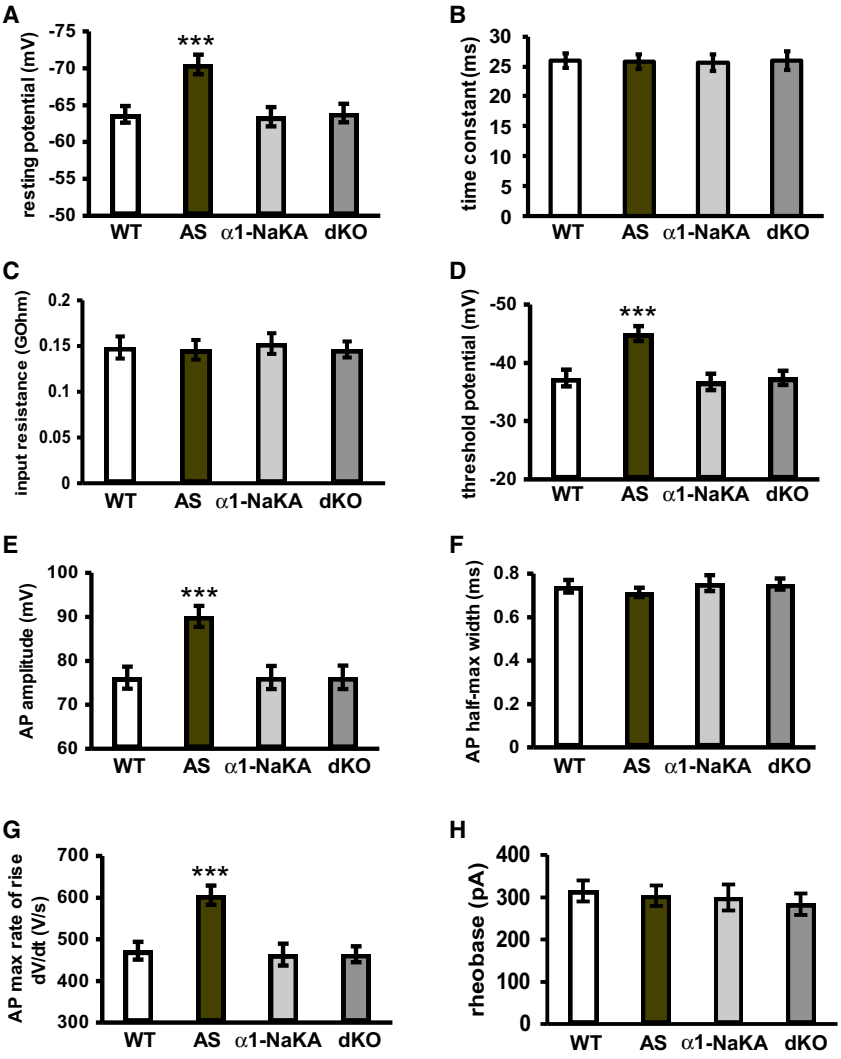

Figure 3. Genetic Reduction of α1-NaKA Corrected Alterations in the Intrinsic Membrane Properties of Hippocampal CA1 Pyramidal Neurons in AS Model Mice

(A–H) Intrinsic membrane properties of hippocampal CA1 pyramidal neurons in WT, AS, α1-NaKA heterozygous knockout (α1-NaKA), and dKO mice measured by current clamp without current injection (I = 0).

(A) Resting membrane potential.

(B) Membrane time constant.

(C) Membrane input resistance.

(D) Threshold potential.

(E) Action potential amplitude.

(F) Action potential full width at half-maximum.

(G) Maximal rate of rise (dV/dt) of the action potential.

(H) Rheobase (amount of current injection needed to induce an action potential at the 5 ms time point).

WT: n = 28 cells, 8 mice; AS: n = 28 cells, 8 mice; α1-NaKA: n = 24 cells, 7 mice; dKO: n = 27 cells, 8 mice. ***$p < 0.001$ (ANOVA). Results are displayed as mean ± SEM. See also Figure S1.

Importantly, genetic reduction of α1-NaKA completely prevented long-term contextual fear memory deficits displayed by the AS mice (Figures 4C and 4D). Likewise, the genetic reduction of α1-NaKA prevented spatial memory deficits displayed by the AS mice in the MWM (Figures 4E and 4F). Escape latency times in the visible platform test were similar for all groups (Figure S3A), as was swim speed (Figure S3B) and distance traveled (Figure S3C). It should be noted that the α1-NaKA heterozygous knockout mice did not display deficits in either contextual fear or spatial memory tests (Figures 4C, 4D, 4E, 4F, and S2C), consistent with previously published behavioral studies of these mice (Lingrel et al., 2007; Moseley et al., 2007). In addition, all groups performed similarly in an open field test (Figures S3D and S3E). Finally, novel object recognition memory, which is context and hippocampus independent (Barker and Warburton, 2011; Forwood et al., 2005; Good et al., 2007; Langston and Wood, 2010), was normal in AS mice and was not altered by the genetic reduction of α1-NaKA (Figure S3F). Taken together, these findings suggest that increased expression of α1-NaKA in the hippocampus during development contributes to long-term hippocampus-dependent memory deficits displayed by AS mice.

DISCUSSION

We previously showed that there is an increase in the expression of α1-NaKA that is correlated with molecular and morphological changes in the AIS, including increased expression of NaV1.6 and ankyrin-G and increased AIS length, in the hippocampus of AS model mice (Kaphzan et al., 2011). We also found that the AS mice exhibited various alterations in intrinsic membrane properties (Kaphzan et al., 2011). Because we found that the increased expression of α1-NaKA in the AS mice is correlated with altered intrinsic membrane properties (Figure S1) and precedes the increases in AIS-related protein levels, we hypothesized that the increase in α1-NaKA levels is the driving force for the alterations in the AIS and intrinsic membrane properties.

Consistent with our hypothesis, we found that genetically reducing the level of α1-NaKA in the AS mice corrected multiple AIS phenotypes in the hippocampus. The increase in expression of the AIS-related proteins NaV1.6 and ankyrin-G in the AS mice was reduced to wild-type levels (Figure 1). In addition, the increase in AIS length in areas CA1 and CA3 of the AS mice was decreased to the length observed in wild-type mice in the dKO mice (Figure 2). Moreover, the altered intrinsic membrane properties in the AS mice that are related to AIS composition and morphology were corrected to those observed in wild-type mice (Figure 3). Taken together, these findings are consistent with the notion that the increased expression of α1-NaKA is one of the events early in development that causes AIS pathology and altered intrinsic membrane properties in AS model mice.

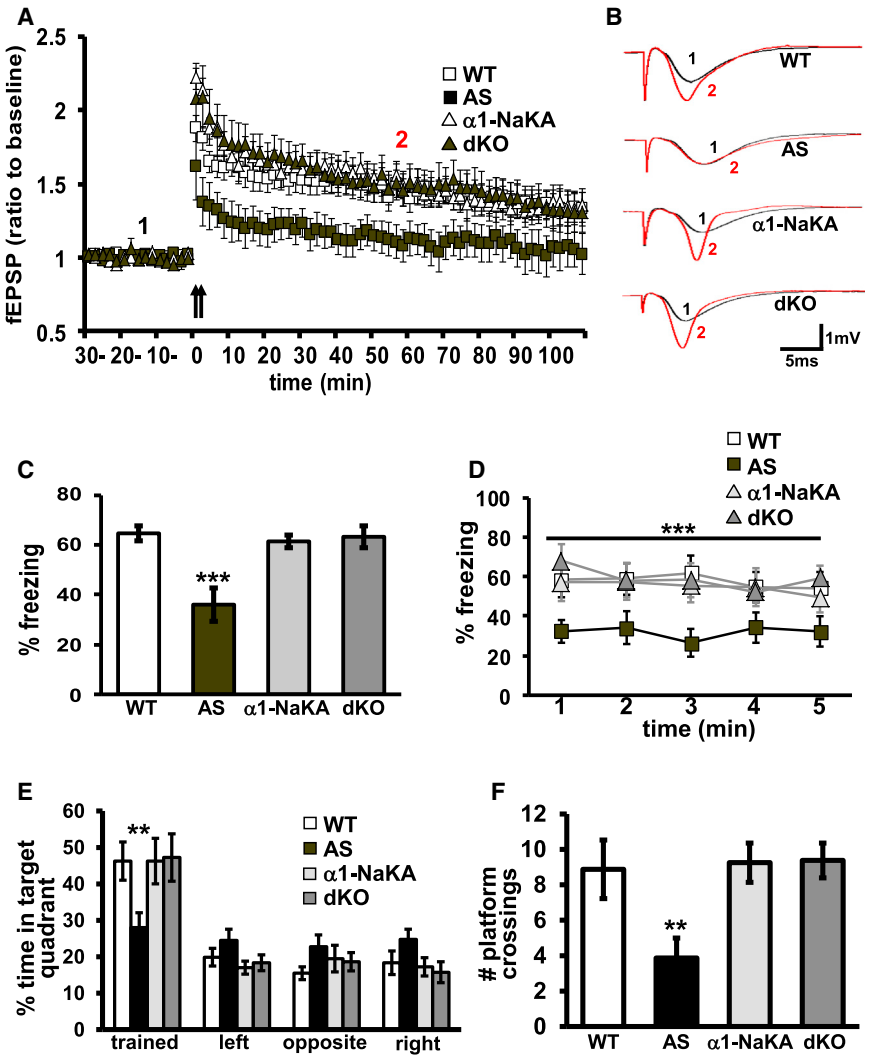

Figure 4. Genetic Reduction of α1-NaKA Corrects Deficits in Hippocampal LTP, Contextual Fear Memory, and Spatial Memory Displayed by AS Mice

(A) Hippocampal slices from WT, AS, α1-NaKA heterozygous knockout mice (α1-NaKA) and dKO mice were stimulated with two trains of high-frequency stimulation (HFS, indicated by the arrows). WT: n = 10 slices, 5 mice; AS: n = 10 slices, 5 mice; α1-NaKA: n = 10 slices, 5 mice; dKO: n = 16 slices, 8 mice. $p < 0.05$ for group, $p < 0.0001$ for time, and $p < 0.0001$ for interaction (RM-ANOVA).

(B) Sample traces of typical field excitatory post-synaptic potentials (fEPSPs) recorded before (black) and 60 min after (red) HFS.

(C) Mice were trained using a standard contextual fear conditioning paradigm and tested for long-term memory measured as % time freezing seven days after training. WT: n = 12 mice; AS: n = 11 mice; α1-NaKA: n = 11 mice; dKO: n = 11 mice. Results are displayed as the average of percent freezing during the entire 5 min test. ***$p < 0.001$ (ANOVA followed by Tukey's post-hoc test).

(D) Results are displayed as percent freezing along the entire test, minute by minute. ***$p < 0.001$ for interaction of group and treatment (RM-ANOVA).

(E) Mice were trained using a standard Morris water maze paradigm and tested for spatial memory of platform location in the probe test (platform removed). n = 8 for WT, AS, and dKO; n = 5 for α1-NaKA. Results are displayed as percentage of time spent in each quadrant along the entire probe test (quadrant time occupancy). $p < 0.05$ for interaction of genotype and quadrant (two-way ANOVA); **$p < 0.01$ for the trained quadrant (Bonferroni post-hoc test).

(F) Results are displayed as a number of platform location crosses during the probe test. **$p < 0.01$ (ANOVA followed by Tukey's post-hoc test).

Results are displayed as mean ± SEM. See also Figures S2 and S3.

The mechanism by which the genetic reduction of α1-NaKA prevents the increased expression of the AIS-related proteins and the abnormal AIS morphology in the absence of E6-AP activity remains unresolved; however, several mechanisms can be considered. It previously was shown that ablating presynaptic input, which induces a decrease in neuronal excitability, results in AIS alterations that resemble the alterations we observed in the AS mice hippocampus (Kuba et al., 2010). These AIS alterations were hypothesized to be feedback responses that normalize overall neuronal excitability, consistent with the homeostatic model of the neuron (Turrigiano and Nelson, 2004). In the AS mice, the increased expression of α1-NaKA would be predicted to decrease excitability by inducing hyperpolarization. Thus, decreased excitability in the AS mice could trigger the observed compensatory changes in the AIS that are aimed at increasing excitability. However, other mechanisms also are possible, such as changes in signal transduction cascades that could result in altered expression of various proteins (Figure 1) or altered network plasticity in AS mice that are restored by reducing α1-NaKA (Figure 4). Future studies in AS mice are needed to further dissect these potential mechanisms.

We believe the current study is important beyond its relevance to AS because it broadens our understanding of AIS plasticity. These studies demonstrate that a genetic manipulation can induce long-term structural plasticity of the AIS. Furthermore, our studies suggest a potential mechanism by which a single molecular change, increased α1-NaKA expression, can induce AIS alterations similar to those observed by blocking presynaptic input (Kuba et al., 2010). Thus, the demonstration that increased expression of α1-NaKA can alter AIS structure and function adds another tier to our understanding of AIS plasticity.

In addition to the correction of abnormalities in the AIS and intrinsic membrane properties, we demonstrated that impaired hippocampal LTP and hippocampus-dependent memory deficits also were corrected by genetically reducing α1-NaKA expression in the AS mice (Figure 4). Whether the correction of the synaptic plasticity and memory deficits is the consequence of reversing the AIS pathology and/or alterations in intrinsic

membrane properties remains to be determined. α1-NaKA is a molecule that is localized in multiple subcellular compartments and affects numerous cellular functions. Hence, it also is possible that the increase in α1-NaKA expression in the AS mice is a key event related to hippocampal deficits via molecular and cellular alterations other than the AIS. Alternatively, it also is possible that the reduction of α1-NaKA expression rescues hippocampal deficits in the AS mice via a different compensatory mechanism.

The clinical significance of the results reported here may extend beyond AS to other classes of psychiatric and developmental disorders. There are a number of studies in the clinical literature that link various psychiatric disorders to either NaKA activity or expression (Al-Mosalem et al., 2009; Chetcuti et al., 2008; Corti et al., 2011; Goldstein et al., 2006; Ji et al., 2009). Furthermore, AIS-specific changes have been identified in superficial pyramidal neurons in postmortem analysis of tissue from human subjects with schizophrenia (Cruz et al., 2009). Thus, it is possible that alterations in neuronal excitability and the AIS in animal models of multiple psychiatric disorders previously were overlooked and now should be examined. Such studies may improve our understanding of neuropsychiatric pathology and suggest additional therapeutic approaches for these disorders.

EXPERIMENTAL PROCEDURES

Mice

Mice for experiments were bred from a female that was heterozygous for the deletion of *Ube3a* from a paternal origin (*Ube3a*$^{p-/m+}$) and an α1-NaKA heterozygous male (α1-NaKA$^{p-/m+}$). Both parents were on a C57/Bl6 background. For all experiments, mice used were 8–12 weeks of age (unless otherwise specified), and for all experiments littermates were used as controls. Mice were genotyped using specific primers as described previously (Jiang et al., 1998; James et al., 1999). All mice were housed in the Transgenic Mouse Facility of New York University, compliant with the *NIH Guide for Care and Use of Laboratory Animals*. Mice were kept on a 12 hr light/dark cycle, with food pellets and water ad libitum.

Tissue Preparation for Western Blots

Mice were decapitated, the brain was quickly extracted, and hippocampi from both hemispheres were removed in an ice-cold cutting solution (CS) containing (in mM) 110 sucrose, 60 NaCl, 3 KCl, 1.25 NaH_2PO_4, 28 $NaHCO_3$, 0.5 $CaCl_2$, 7 $MgCl_2$, 5 glucose, and 0.6 ascorbate, and immediately snap-frozen on dry ice. Frozen hippocampi were placed in ice-cold lysis buffer containing (in mM) 40 HEPES (pH 7.5), 150 NaCl, 10 pyrophosphate, 10 glycerophosphate, 1 EDTA and 0.3% CHAPS, and protease inhibitor (Protease Inhibitor II and Phosphatase Inhibitor Cocktail I, II [Sigma]) and homogenized by sonication. Protein quantification was carried out with bicinchoninic acid protein assay reagent (Thermo Scientific).

Western Blots

After homogenization and protein quantification, protein samples were added to β-mercaptoethanol-containing SDS sample buffer and heated for 2 min in 60°C prior to loading on SDS-polyacrylamide gels. After heating the samples, 4–20 μg of protein (depending on the specific protein and the linear range of detection) were loaded on 4%–12% gradient SDS-PAGE gels, resolved, transferred to polyvinylidene fluoride membranes, and probed with primary antibodies using standard techniques. The primary antibodies and the dilutions for the western blots used in these studies are as follows: NaV1.6 1:500 (Sigma-Aldrich); α1-NaKA (clone C464.6) 1:1,000 (Millipore); ankyrin-G 1:1,000, β-actin and GAPDH 1:5,000 (Santa Cruz Biotechnology). Secondary antibodies were conjugated with horseradish peroxidase. All blots were developed using enhanced chemiluminescence detection (GE Healthcare). The bands of each western blot were imaged and quantified using the KODAK 4000MM imaging system. All signals were obtained in the linear range for each antibody, normalized by total protein, and quantified via densitometry. Data represent mean ±SEM. ANOVA was used for western blot analysis with $p < 0.05$ as significance criteria.

Intracellular Electrophysiology

Brains from the four mouse genotypes were quickly removed and transverse hippocampal slices (300 μm) were isolated with a Leica VT1200 Vibratome (Leica). Slices were cut in ice-cold cutting solution containing (in mM) 110 sucrose, 60 NaCl, 3 KCl, 1.25 NaH_2PO_4, 28 $NaHCO_3$, 0.5 $CaCl_2$, 7 $MgCl_2$, 5 glucose, and 0.6 ascorbate. Slices were recovered for 45 min at 36°C in artificial cerebrospinal fluid (ACSF) containing (in mM) 125 NaCl, 2.5 KCl, 1.25 NaH_2PO_4, 25 $NaHCO_3$, 25 D-glucose, 2 $CaCl_2$, and 1 $MgCl_2$ ACSF, followed by additional recovery for 30 min in room-temperature ACSF. After initial recovery, slices were placed in a submerged chamber and maintained at 36°C in ACSF (2 ml/min). Slices were allowed to recover for an additional 60 min on the electrophysiology rig prior to experimentation. All solutions were constantly caboxygenated with 95% O_2 + 5% CO_2. Hippocampal CA1 pyramidal cells were illuminated and visualized using a ×60 water-immersion objective mounted on a fixed-stage microscope (BX51-WI; Olympus), and the image was displayed on a video monitor using a charge-coupled device camera (Hamamatsu). Recordings were amplified by multiclamp 700B and digitized by Digidata 1440 (Molecular Devices). The recording electrode was pulled from a borosilicate glass pipette (3–5 MΩ) using an electrode puller (P-97; Sutter Instruments) and filled with a K-gluconate-based internal solution containing (in mM) 120 K-gluconate, 20 KCl, 10 HEPES, 2 MgCl2, 4 Na2ATP, 0.5 TrisGTP, 14 phosphocreatine, osmolarity 290 mOsm, and pH 7.3. The recording glass pipettes were patched onto the CA1 pyramidal cells soma region. Voltages for liquid junction potential (+14 mV) were not corrected online. All current-clamp recordings were low-pass filtered at 10 kHz and sampled at 50 kHz. Series resistance was compensated and only series resistance <20 MΩ was included in the data set. Pipette capacitance was ~99% compensated. The method for measuring active intrinsic properties was based on a modified version of Kole and Stuart (2008). After initial assessment of the current, which was required to induce an action potential at 15 ms from the start of the current injection with large steps (50 pA), we injected a series of brief depolarizing currents for 10 ms in steps of 10 pA increments. The first action potential that appeared on the 5 ms time point was analyzed. A curve of dV/dt was created for that trace, and threshold was considered as the 30 V/s point in the rising slope of the action potential. Series resistance, input resistance, and membrane capacitance were monitored during the entire experiment. Changes in these parameters (which were monitored throughout the entire duration of the experiment) bigger than 10% were criteria for exclusion of data. Data analysis was done with Clampfit (Molecular Devices, Sunnyvale, CA). ANOVA was used for electrophysiological data analysis with $p < 0.05$ as significance criteria.

Extracellular Electrophysiology

Hippocampal slices were prepared using the same procedure used for whole-cell recordings, except that the slice thickness was altered (400 μm). Slices were allowed to recover for 20 min at room temperature in 50:50 CS:ACSF containing (in mM) 125 NaCl, 2.5 KCl, 1.25 NaH_2PO_4, 25 $NaHCO_3$, 25 D-glucose, 2 $CaCl_2$, and 1 $MgCl_2$ ACSF, followed by additional recovery for 30 min in room-temperature ACSF. After initial recovery, slices were placed in an interface chamber (Scientific Systems Design) and maintained at 33°C in ACSF (2 ml/min). Slices were allowed to recover for an additional 120 min on the electrophysiology rig prior to experimentation. All solutions were constantly caboxygenated with 95% O_2 + 5% CO_2. Bipolar stimulating electrodes (92:8 Pt:Y) were placed at the border of area CA3 and area CA1 along the Schaffer-Collateral pathway. ACSF-filled glass recording electrodes (1–3 MΩ) were placed in stratum radiatum of area CA1. Basal synaptic transmission was assessed for each slice by applying gradually increasing stimuli (0.5–15V) using a stimulus isolator (A-M Systems) and determining the input:output relationship. All subsequent stimuli applied to slices was equivalent to the level necessary to evoke a field excitatory postsynaptic potential (fEPSP) that was

25%–35% of the maximal initial slope that could be evoked. Synaptic efficacy was continuously monitored (0.05 Hz). Sweeps were averaged together every 2 min. fEPSPs were amplified (A-M Systems Model 1800) and digitized (Digidata 1440; Molecular Devices) prior to analysis (pClamp; Molecular Devices). Stable baseline synaptic transmission was established for at least 60 min. Slices were given high-frequency stimulation (HFS) to induce LTP using two trains of 100 Hz for 1 s, with an interval of 20 s between each train. Stimulus intensity of the HFS was matched to the intensity used in the baseline recordings. The initial slopes of the fEPSPs from averaged traces were normalized to those recorded during baseline. RM-ANOVAs were used for electrophysiological data analysis with $p < 0.05$ as significance criteria.

Contextual Fear Conditioning

Mice were handled for 3 consecutive days (10 min/day) prior to experimentation. On the day of the behavioral assays, the mice were habituated for at least 30 min to the testing room. On the conditioning day, each mouse was placed in the chamber and received two foot-shocks (0.5 mA intensity, 2 s duration, 1 min interval) starting after 2 min of free exploration. The contextual memory test was performed 7 days later by placing each mouse back into the same conditioning chamber for 5 min. Freezing behavior, defined as a lack of movement except those involved in respiration, was measured using video files that were analyzed by an observer blind to mouse genotype and treatment. Freezing behavior during conditioning was assessed four times during the 5 min period: 2 min exploration before the first shock and then every minute interval (i.e., after the first foot shock, after the second foot shock, and during the last minute). Freezing behavior during contextual memory test was assessed every minute along the 5 min period. Freezing time was converted to percent freezing by the formula [duration of freezing (s) in the time interval/time of the interval (s)] × 100. Data were analyzed with repeated-measure ANOVA, using either time or interval as the within-subject factor and genotype and treatment as the between-subject variable. ANOVA was used to analyze the total average percent freezing during the contextual memory test.

Immunostaining

Mice were deeply anesthetized with isoflurane before transcardial perfusion with ice-cold 4% PFA in 0.1M Na-phosphate buffer (PB; pH 7.2). Brains were postfixed in 4% PFA 0.1M PB for 1 hr and equilibrated in 20% sucrose 0.1M PB over 48 hr. Afterward, 25 μm coronal slices containing the hippocampal formation were cut on a microtome and washed in 0.1M PB. Slices were mounted on gelatin-coated coverslips, then blocked in 10% normal goat serum 0.1M PB containing 0.3% TX-100 (PBTgs). Tissue was incubated overnight at 4°C in primary antibodies diluted in PBTgs. Primary antibodies were removed by washing the tissue 3 times for 5 min with PBTgs. Alexa594-conjugated goat anti-mouse (1:1,000) secondary antibodies diluted in PBTgs were applied for 1 hr at RT and used to visualize primary antibodies. Fluorescent dye-conjugated secondary antibodies were purchased from Invitrogen. Excess secondary antibodies were removed by consecutive 5 min washes with PBTgs, 0.1 M PB, and 0.05 M PB. Fluorescence imaging was performed on an AxioImager Z1 microscope (Carl Zeiss MicroImaging) fitted with an AxioCam digital camera (Carl Zeiss MicroImaging). AxioVision acquisition software (Carl Zeiss MicroImaging) was used for collection of images. Comparison of wild-type and AS tissue was performed on slices prepared in parallel and images were acquired at identical exposure times. Experiments were performed at least in triplicate. Fluorescence intensity was measured using ImageJ (NIH). No additional processing of images was performed.

Antibodies for Immunostaining

The primary antibody that was used is mouse anti-ankyrin-G (NeuroMab, clone N106/36). Alexa Fluor 594-conjugated goat anti-mouse secondary antibodies (Invitrogen) were used to visualize the ankyrin-G antibodies.

AIS Length Quantification

AIS length was determined by line-scan length quantification of ankyrin-G immunosignal in Image J (NIH). For quantification, we measured the length of AIS contained within either a single image plane or through three-dimensional space in consecutive z stack images. Anti- ankyrin-G immunosignal was uniformly distributed throughout the AIS, providing a stark contrast in fluorescence intensity values at the axon hillock to AIS and AIS to distal axon transitions. Thus, to determine AIS length, we generated fluorescence intensity plots of ankyrin-G immunoreactivity and calculated the first derivative of the resulting intensity curve. The start and end points of the AIS were defined as the maximum and minimum values, respectively, of the derivative curve.

Statistical Analysis

ANOVA (one way and repeated measures) were used where appropriate. Results are displayed as mean ± SEM.

For further details, please refer to the Extended Experimental Procedures.

SUPPLEMENTAL INFORMATION

Supplemental Information includes Extended Experimental Procedures and three figures and can be found with this article online at http://dx.doi.org/10.1016/j.celrep.2013.07.005.

ACKNOWLEDGMENTS

This work was supported by National Institutes of Health grants NS034007, NS047384, and NS078718 (E.K.), NS044916 (M.N.R.), and NS073295 (S.A.B.) and by the Angelman Syndrome Foundation (E.K).

Received: January 13, 2013
Revised: May 9, 2013
Accepted: July 3, 2013
Published: August 1, 2013

REFERENCES

Al-Mosalem, O.A., El-Ansary, A., Attas, O., and Al-Ayadhi, L. (2009). Metabolic biomarkers related to energy metabolism in Saudi autistic children. Clin. Biochem. *42*, 949–957.

Barker, G.R., and Warburton, E.C. (2011). When is the hippocampus involved in recognition memory? J. Neurosci. *31*, 10721–10731.

Brodie, C., Bak, A., Shainberg, A., and Sampson, S.R. (1987). Role of Na-K ATPase in regulation of resting membrane potential of cultured rat skeletal myotubes. J. Cell. Physiol. *130*, 191–198.

Chetcuti, A., Adams, L.J., Mitchell, P.B., and Schofield, P.R. (2008). Microarray gene expression profiling of mouse brain mRNA in a model of lithium treatment. Psychiatr. Genet. *18*, 64–72.

Corti, C., Xuereb, J.H., Crepaldi, L., Corsi, M., Michielin, F., and Ferraguti, F. (2011). Altered levels of glutamatergic receptors and Na+/K+ ATPase-α1 in the prefrontal cortex of subjects with schizophrenia. Schizophr. Res. *128*, 7–14.

Cruz, D.A., Weaver, C.L., Lovallo, E.M., Melchitzky, D.S., and Lewis, D.A. (2009). Selective alterations in postsynaptic markers of chandelier cell inputs to cortical pyramidal neurons in subjects with schizophrenia. Neuropsychopharmacology *34*, 2112–2124.

Forwood, S.E., Winters, B.D., and Bussey, T.J. (2005). Hippocampal lesions that abolish spatial maze performance spare object recognition memory at delays of up to 48 hours. Hippocampus *15*, 347–355.

Gadsby, D.C. (1984). The Na/K pump of cardiac cells. Annu. Rev. Biophys. Bioeng. *13*, 373–398.

Goldstein, I., Levy, T., Galili, D., Ovadia, H., Yirmiya, R., Rosen, H., and Lichtstein, D. (2006). Involvement of Na(+), K(+)-ATPase and endogenous digitalis-like compounds in depressive disorders. Biol. Psychiatry *60*, 491–499.

Good, M.A., Barnes, P., Staal, V., McGregor, A., and Honey, R.C. (2007). Context- but not familiarity-dependent forms of object recognition are impaired following excitotoxic hippocampal lesions in rats. Behav. Neurosci. *121*, 218–223.

James, P.F., Grupp, I.L., Grupp, G., Woo, A.L., Askew, G.R., Croyle, M.L., Walsh, R.A., and Lingrel, J.B. (1999). Identification of a specific role for the

Na,K-ATPase alpha 2 isoform as a regulator of calcium in the heart. Mol. Cell *3*, 555–563.

Ji, L., Chauhan, A., Brown, W.T., and Chauhan, V. (2009). Increased activities of Na+/K+-ATPase and Ca2+/Mg2+-ATPase in the frontal cortex and cerebellum of autistic individuals. Life Sci. *85*, 788–793.

Jiang, Y.H., Armstrong, D., Albrecht, U., Atkins, C.M., Noebels, J.L., Eichele, G., Sweatt, J.D., and Beaudet, A.L. (1998). Mutation of the Angelman ubiquitin ligase in mice causes increased cytoplasmic p53 and deficits of contextual learning and long-term potentiation. Neuron *21*, 799–811.

Kaphzan, H., Buffington, S.A., Jung, J.I., Rasband, M.N., and Klann, E. (2011). Alterations in intrinsic membrane properties and the axon initial segment in a mouse model of Angelman syndrome. J. Neurosci. *31*, 17637–17648.

Kishino, T., Lalande, M., and Wagstaff, J. (1997). UBE3A/E6-AP mutations cause Angelman syndrome. Nat. Genet. *15*, 70–73.

Knoll, J.H., Nicholls, R.D., Magenis, R.E., Graham, J.M., Jr., Lalande, M., and Latt, S.A. (1989). Angelman and Prader-Willi syndromes share a common chromosome 15 deletion but differ in parental origin of the deletion. Am. J. Med. Genet. *32*, 285–290.

Kole, M.H., and Stuart, G.J. (2008). Is action potential threshold lowest in the axon? Nat. Neurosci. *11*, 1253–1255.

Kuba, H., Oichi, Y., and Ohmori, H. (2010). Presynaptic activity regulates Na(+) channel distribution at the axon initial segment. Nature *465*, 1075–1078.

Langston, R.F., and Wood, E.R. (2010). Associative recognition and the hippocampus: differential effects of hippocampal lesions on object-place, object-context and object-place-context memory. Hippocampus *20*, 1139–1153.

Lingrel, J.B., Williams, M.T., Vorhees, C.V., and Moseley, A.E. (2007). Na,K-ATPase and the role of alpha isoforms in behavior. J. Bioenerg. Biomembr. *39*, 385–389.

Lossie, A.C., Whitney, M.M., Amidon, D., Dong, H.J., Chen, P., Theriaque, D., Hutson, A., Nicholls, R.D., Zori, R.T., Williams, C.A., and Driscoll, D.J. (2001). Distinct phenotypes distinguish the molecular classes of Angelman syndrome. J. Med. Genet. *38*, 834–845.

Mallick, B.N., Singh, S., and Singh, A. (2010). Mechanism of noradrenaline-induced stimulation of Na-K ATPase activity in the rat brain: implications on REM sleep deprivation-induced increase in brain excitability. Mol. Cell. Biochem. *336*, 3–16.

Matsuura, T., Sutcliffe, J.S., Fang, P., Galjaard, R.J., Jiang, Y.H., Benton, C.S., Rommens, J.M., and Beaudet, A.L. (1997). De novo truncating mutations in E6-AP ubiquitin-protein ligase gene (UBE3A) in Angelman syndrome. Nat. Genet. *15*, 74–77.

Moseley, A.E., Williams, M.T., Schaefer, T.L., Bohanan, C.S., Neumann, J.C., Behbehani, M.M., Vorhees, C.V., and Lingrel, J.B. (2007). Deficiency in Na,K-ATPase alpha isoform genes alters spatial learning, motor activity, and anxiety in mice. J. Neurosci. *27*, 616–626.

Silva, E., Gomes, P., and Soares-da-Silva, P. (2006). Overexpression of Na(+)/K (+)-ATPase parallels the increase in sodium transport and potassium recycling in an in vitro model of proximal tubule cellular ageing. J. Membr. Biol. *212*, 163–175.

Sutcliffe, J.S., Jiang, Y.H., Galijaard, R.J., Matsuura, T., Fang, P., Kubota, T., Christian, S.L., Bressler, J., Cattanach, B., Ledbetter, D.H., and Beaudet, A.L. (1997). The E6-Ap ubiquitin-protein ligase (UBE3A) gene is localized within a narrowed Angelman syndrome critical region. Genome Res. *7*, 368–377.

Turrigiano, G.G., and Nelson, S.B. (2004). Homeostatic plasticity in the developing nervous system. Nat. Rev. Neurosci. *5*, 97–107.

van Woerden, G.M., Harris, K.D., Hojjati, M.R., Gustin, R.M., Qiu, S., de Avila Freire, R., Jiang, Y.H., Elgersma, Y., and Weeber, E.J. (2007). Rescue of neurological deficits in a mouse model for Angelman syndrome by reduction of alphaCaMKII inhibitory phosphorylation. Nat. Neurosci. *10*, 280–282.

Williams, C.A., Beaudet, A.L., Clayton-Smith, J., Knoll, J.H., Kyllerman, M., Laan, L.A., Magenis, R.E., Moncla, A., Schinzel, A.A., Summers, J.A., and Wagstaff, J. (2006). Angelman syndrome 2005: updated consensus for diagnostic criteria. Am. J. Med. Genet. A. *140*, 413–418.